Ma et al. Journal of Translational Medicine (2024) 22:834
https://doi.org/10.1186/s12967-024-05636-3

Journal of Translational Medicine

RESEARCH Open Access

USP14 inhibition promotes DNA damage repair and represses ovarian granulosa cell senescence in premature ovarian insufficiency

Lin-Zi Ma[1†], Ao Wang[1†], Yun-Hui Lai[1], Jun Zhang[1], Xiao-Fei Zhang[1], Shi-Ling Chen[1*] and Xing-Yu Zhou[1,2*]

Abstract

Background Premature ovarian insufficiency (POI) is a condition characterized by a substantial decline or loss of ovarian function in women before the age of 40. However, the pathogenesis of POI remains to be further elucidated, and specific targeted drugs which could delay or reverse ovarian reserve decline are urgently needed. Abnormal DNA damage repair (DDR) and cell senescence in granulosa cells are pathogenic mechanisms of POI. Ubiquitin-specific protease 14 (USP14) is a key enzyme that regulates the deubiquitylation of DDR-related proteins, but whether USP14 participates in the pathogenesis of POI remains unclear.

Methods We measured USP14 mRNA expression in granulosa cells from biochemical POI (bPOI) patients. In KGN cells, we used IU1 and siRNA-USP14 to specifically inhibit USP14 and constructed a cell line stably overexpressing USP14 to examine its effects on DDR function and cellular senescence in granulosa cells. Next, we explored the therapeutic potential of IU1 in POI mouse models induced by D-galactose.

Results USP14 expression in the granulosa cells of bPOI patients was significantly upregulated. In KGN cells, IU1 treatment and siUSP14 transfection decreased etoposide-induced DNA damage levels, promoted DDR function, and inhibited cell senescence. USP14 overexpression increased DNA damage, impaired DDR function, and promoted cell senescence. Moreover, IU1 treatment and siUSP14 transfection increased nonhomologous end joining (NHEJ), upregulated RNF168, Ku70, and DDB1, and increased ubiquitinated DDB1 levels in KGN cells. Conversely, USP14 overexpression had the opposite effects. Intraperitoneal IU1 injection alleviated etoposide-induced DNA damage in granulosa cells, ameliorated the D-galactose-induced POI phenotype, promoted DDR, and inhibited cell senescence in ovarian granulosa cells in vivo.

Conclusions Upregulated USP14 in ovarian granulosa cells may play a role in POI pathogenesis, and targeting USP14 may be a potential POI treatment strategy. Our study provides new insights into the pathogenesis of POI and a novel POI treatment strategy.

[†]Lin-Zi Ma and Ao Wang contributed equally to this work.

*Correspondence:
Shi-Ling Chen
chensl_92@vip.163.com
Xing-Yu Zhou
zhouxy315@163.com

Full list of author information is available at the end of the article

Keywords Premature ovarian insufficiency, Granulosa cells, Ubiquitin-specific protease 14, DNA damage repair, Cell senescence

Background

Premature ovarian insufficiency (POI), formerly known as premature ovarian failure (POF), is a condition characterized by a substantial decline or loss of ovarian function in women before the age of 40. The subtle onset and imperceptible development of POI make early diagnosis difficult; that is, the ovarian function of most POI patients is greatly impaired at diagnosis [1]. Moreover, there is no effective treatment to delay or reverse ovarian reserve decline. Only long-term regular hormone replacement therapy can be used to prevent and treat the symptoms of estrogen deficiency, maintain the patient's health and prevent long-term complications [2]. Therefore, the pathogenesis of POI remains to be further elucidated, and developing specific targeted drugs is urgently needed.

Recent studies have reported that dysfunction in DNA damage repair (DDR) plays an important role in the pathogenesis of POI [3]. Some mutations in the genes related to the DDR, including MCM8, MCM9, MSH5 and FANCA, can directly impede oocyte meiosis, affect follicle development, and accelerate follicle depletion, eventually leading to the development of POI [4]. In addition, abnormal regulation of DDR-associated genes in granulosa cells has also been highlighted by recent studies. Aberrant expression of several noncoding RNAs, such as long noncoding RNA HCP5 [5], long noncoding RNA DDGC [6], microRNA-379-5p [7] and microRNA-127-5p [8], was detected in granulosa cells of patients with biochemical POI (bPOI) and had deleterious effects on DDR function.

Normal DDR function is essential to maintain cell genomic stability. Dysfunction of the DDR may not only induce programmed cell death but also lead to cell senescence [9]. Once the DDR pathway is activated, the cell cycle is blocked, sequentially promoting DDR progression. However, the persistence of DNA damage and the subsequent continuous activation of DDR signaling can stall cell proliferation and induce cellular senescence [10]. Recent studies have also suggested that premature senescence of ovarian tissue cells, especially granulosa cells, may play an important role in the pathogenesis of POI, but the mechanism of granulosa cell senescence has not been fully clarified [11, 12]. Furthermore, drugs targeting cell senescence and DDR progression in granulosa cells may be effective for the treatment of POI [13].

Ubiquitin-specific protease 14 (USP14), a deubiquitinating enzyme (DUB), plays a major role in negatively regulating ubiquitination modifications by releasing ubiquitin molecules from substrates and allosterically regulating the 26 S proteasome complex [14]. As ubiquitin modifications play important roles in maintaining protein stability, regulating protein molecule interactions, and modulating protein activity, USP14 is involved in a variety of physiological processes and disease pathogenesis by affecting the stability and function of many proteins [15]. In particular, recent studies have indicated that USP14 is a key enzyme in regulating the deubiquitination of DDR proteins. Sharma A et al. reported that when cellular autophagy is inhibited, USP14 accumulates intracellularly and then antagonizes the RNF168-dependent K13/K15 ubiquitination of H2A and ubiquitin–proteasome degradation of the RNF168 protein [16]. In the nonhomologous end joining (NHEJ) repair process, the Ku70/Ku80 complex recognizes and binds to broken DNA ends and subsequently recruits DNA-PKcs and downstream DDR factors. When cellular autophagy is inhibited, upregulated USP14 promotes Ku70 deubiquitination, leading to a decrease in the ability of Ku70 to bind to DSB sites, and thus arresting the progression of NHEJ [17]. In non-small cell lung cancer, inhibition of USP14 expression increased radiotherapy sensitivity, as indicated by an increase in NHEJ activity and a decrease in homologous recombination (HR) [18]. The above studies indicate that USP14 is a key enzyme in regulating the deubiquitination of NHEJ pathway molecules, but whether it plays a similar role in ovarian granulosa cells and is involved in the pathogenesis of POI is still unclear.

A USP14 specific inhibitor, IU1, blocks the USP14 function via a steric blockade mechanism. The two surface loops of free USP14, blocking loop 1 (BL1) and BL2, partially hover above, to block the binding of the active site of USP14 cleft to the C-terminus of ubiquitin and maintain the autoinhibited state of USP14. When USP14 interacts with the 26 S proteasome, the BL1 and BL2 loops move away from the active site of USP14, activating its deubiquitinating function. IU1 has a binding pocket structure only 8.3 Å away from the USP14 catalytic center Cys114, which allows it to bind competitively with the ubiquitin C-terminus to the catalytic active site of USP14 through a steric blockade mechanism [15]. Due to the crucial role of USP14 in the pathogenesis of many diseases, several studies have focused on the therapeutic role of IU1 [19]. Therefore, we further explored the therapeutic potential of IU1 in POI mouse models induced by D-galactose (D-gal).

In the present study, we measured the expression of USP14 mRNA in the granulosa cells of patients with bPOI and further investigated the molecular mechanism by which USP14 impairs DDR and promotes cell

senescence in ovarian granulosa cells, aiming to clarify the role of USP14 in the pathogenesis of POI. More importantly, we discovered a new potential therapeutic approach for POI through the study of USP14 in granulosa cells. In our study, we demonstrated that IU1 could ameliorate etoposide (ETO)-induced DNA damage in granulosa cells in vivo and in vitro and improve the D-gal-induced senescence phenotype in POI model mice.

Materials and methods

Patient inclusion criteria and human luteinized granulosa cell (hLGC) collection

The study was approved by the Ethics Committee of Nanfang Hospital, Southern Medical University (NFEC-2017–197), and was carried out in accordance with the Declaration of Helsinki. After obtaining written informed consent from patients, a total of 50 patients with bPOI as the bPOI group and 41 patients who were treated with in vitro fertilization/intracytoplasmic sperm injection-embryo transfer (IVF/ICSI-ET) for male or tubal factors as the control group were recruited from the Center for Reproductive Medicine, Department of Gynecology and Obstetrics, Nanfang Hospital, Southern Medical University, from January 2017 to December 2020. The inclusion criteria of bPOI patients included ≤ 39 years of age, and at least one of the following conditions were met: (1) basal serum follicle-stimulating hormone (FSH) ≥ 10 mIU/ml on two occasions > 4 weeks apart, (2) bilateral ovarian antral follicle count (AFC) ≤ 5, and (3) anti-Müllerian hormone (AMH) ≤ 1.1 ng/mL. The inclusion criteria of control patients were (1) ≤ 39 years of age, (2) basal FSH < 10 mIU/ml on two occasions > 4 weeks apart, (3) bilateral AFC > 5, and (4) serum AMH > 1.1 ng/mL. Exclusion criteria included karyotype abnormalities, a history of ovarian surgery, a history of radiotherapy or chemotherapy, and a history of other reproductive endocrine disorders, such as polycystic ovary syndrome (PCOS), hyperprolactinemia, endometriosis, or hypogonadotropic amenorrhea.

hLGCs were collected from the discarded follicular fluid of the patient during IVF/ICSI-ET through density gradient centrifugation with Percoll Cell Separation Solution (GE HealthCare, Chicago, IL, USA), as described in our previous study [20]. After centrifugation, the supernatant was removed, and 1 mL of RNAiso Plus (TaKaRa Bio, Dalian, China) was added to the cell precipitate, mixed well, placed at room temperature for 5 min, and then stored at -80 °C until RNA extraction.

RNA isolation and quantitative real-time polymerase chain reaction (qRT–PCR)

Total RNA was extracted using RNAiso Plus (TaKaRa) and then converted to cDNA using the PrimeScipt RT reagent kit (TaKaRa). qRT–PCR was performed using Quant Studio 5 (Applied Biosystems, CT, USA) with SYBR Premix Ex Taq II (TaKaRa) according to the manufacturer's instructions. The expression of protein-coding genes was normalized to that of GAPDH, 18 S rRNA and ACTB and calculated by the $2^{-\Delta\Delta CT}$ equation, and the mean was used for calculation. The sequences of primers used are as follows: GAPDH forward 5′-ACCATCTTCC AGGAGCGAGA-3′, GAPDH reverse 5′-GACTCCACG ACGTACTCAGC-3′; and USP14 forward 5′-GCAGTAC TAACACACCAGGGAAGG-3′, USP14 reverse 5′-CTC CACCACCAGAAAGCCGTAAG-3′.

Cell culture and siRNA transfection

KGN and HEK293T cell lines were obtained from Procell Bio (Wuhan, China) and maintained at 37 °C with 5% CO_2 in a cell incubator. KGN cells were cultured in Dulbecco's modified Eagle's medium (DMEM)/F-12 nutrient mixture supplemented with 10% fetal bovine serum (Gibco, Life Technologies, Carlsbad, CA, USA). HEK293T cells were cultured in DMEM (Gibco) with 10% fetal bovine serum (Gibco). Oligonucleotide siRNA duplexes targeting USP14 were synthesized by RiboBio (Guangzhou, China), with sequence of 5′-GGACUUAAA UUGCGACUUCTT-3′. KGN cells were transfected with siRNAs using Lipofectamine 3000 (Life Technologies, Carlsbad, CA, USA).

Lentivirus infections

The lentivirus-mediated vectors with USP14 were established by Hanbio (Shanghai, China). KGN cells in the logarithmic growth phase were inoculated into a six-well plate at a density of 2×10^5 cells/well. When cell confluence reached 50%, a total of 10 MOI of the corresponding lentivirus was added to 1 mL of medium with 12 h of incubation. Puromycin (1 μg/mL) was added to screen the stably transfected cells, and the cells were passaged every 48 h until no cell death was detected. Thereafter, medium with 0.25 μg/mL puromycin was used for maintenance culture.

Plasmid extraction and transfection

Flag-USP14, His-DDB1, HA-ub overexpression and control plasmids were purchased from Hanbio (Shanghai, China). HEK293T cells in the logarithmic growth phase were first digested in trypsin and seeded into 6-cm cell culture dishes. When the cells grew to 50% confluence, they were transiently transfected with different plasmids using Lipofectamine 3000 reagent (Gibco). After 48 h of incubation, the transfected cells were collected for further experiments.

Comet assay

DNA damage in KGN cells was measured using comet assay kits (Keygen, Nanjing, China). Briefly, 1×10^6

isolated cells were mixed with 100 μL of 0.7% low melting point agarose, 100 μL of which was layered on normal agarose slides and solidified under coverslips at 4 °C. After 10 min, the coverslips were removed and placed in lysis buffer for 1 h at 4 °C. Then, the slides were placed in electrophoresis solution (300 mM NaOH, 1 mM EDTA) for 1 h incubation at room temperature, followed by 30 min of electrophoresis (25 V). Next, the slides were immersed in 0.4 mM Tris-HCl (pH 7.5) buffer for 10 min at 4 ℃ three times for neutralization, followed by staining using PI for 10 min protected from light. Images were scanned under an Imager D2 (Zeiss, Oberkochen, Germany) fluorescence microscope, cells were counted using ImageJ, and the DNA tails were analyzed.

Protein extraction and Western blot analysis

KGN cells, HEK293T cells or ovarian tissues were lysed in protein lysis buffer containing ice-cold radioimmunoprecipitation assay (RIPA) buffer (Beyotime, Shanghai, China) supplemented with 1× phenylmethanesulfonyl fluoride (PMSF, Beyotime), 1× protease inhibitor cocktail (Beyotime), and 1× phosphatase inhibitor (Beyotime). The lysates were clarified by centrifugation at 13,000 rpm for 20 min at 4 °C, and then the protein concentration of the supernatant was quantified using a BCA Protein Assay kit (Beyotime). The remaining supernatant plus 1/4 volume of loading buffer was denatured at 100 °C and then frozen at -80 °C for subsequent experiments.

Equal amounts of protein (30 μg) were separated by sodium dodecyl sulfate–polyacrylamide gel electrophoresis (SDS–PAGE) before electro-transfer to polyvinylidene fluoride (PVDF) membranes (Bio-Rad Laboratories, Hercules, CA, USA). After blocking with 5% BSA for 2 h at room temperature, the membranes were incubated overnight at 4 °C with specific primary antibodies. After being washed 3 times with Tris-buffered saline (TBS, Servicebio, Wuhan, China) with 0.1% Tween 20 (TBST) for 10 min, the membranes were incubated with the appropriate secondary antibodies for 1 h at room temperature and then washed again 3 times with TBST. Then, bands were detected by Clarity Western Enhanced Chemiluminescence (ECL) Substrate (Bio-Rad). The band intensity was analyzed and normalized using ImageJ software. The following antibodies were used: γH2AX antibody (CST, USA, 8240, 1:1000 dilution), p21 antibody (CST, 2947, 1:1000 dilution), 53BP1 antibody (Abcam, Cambridge, UK, ab175933, 1:1000 dilution), DDB1 antibody (Abcam, ab109027, 1:1000 dilution), Ku70 antibody (Proteintech, Wuhan, China, 66607-1-Ig, 1:1000 dilution), H2AX antibody (Proteintech, 10856-1-AP, 1:2000 dilution), ubiquitin antibody (Santa Cruz, USA, 1:200 dilution), Flag antibody (Abcam, ab205606, 1:1000 dilution), His antibody (Proteintech, 66005-1-Ig, 1:1000 dilution), cleaved-PARP antibody (Abcam, ab32064, 1:2000 dilution), PCNA antibody (Santa Cruz, sc-56, 1:1000 dilution), β-gal antibody (Santa Cruz, sc-377257, 1:200 dilution), GAPDH antibody (Proteintech, 60004-1-Ig, 1:5000 dilution), and HRP-conjugated secondary antibody (Beyotime, SA00001-1 and SA00002-1, 1:3000 dilution).

Coimmunoprecipitation (Co-IP)

For the co-IP assay, HEK293T cells were gently washed once with PBS. After adding IP lysis buffer (Beyotime) supplemented with 1× PMSF to the dish, the cells were scraped off and collected in a 1.5 mL centrifuge tube. Then, the cells were lysed on ice for 10 min, and the supernatant was collected after centrifugation at 13,000 rpm for 15 min at 4 °C. After washing twice with IP Lysis buffer, Protein A/G immunoprecipitated magnetic beads (Bimake, Houston, TX USA) were added to IP Lysis buffer containing antibody and slowly turned over at room temperature for 15 min to bind the antibody. Then, the beads were magnetically separated and resuspended in the previous supernatant and slowly tumbled overnight at 4 °C. The next day, the beads were washed twice and mixed with loading buffer and heated at 100 °C for 5 min, and the supernatant was collected for Western blotting. The following antibodies were used: His antibody (Proteintech, 66005-1-Ig, 1 μg), Flag antibody (Abcam, ab205606, 1 μg) and ubiquitin antibody (Santa Cruz, sc-8017, 1 μg).

Animals

Female 6-week-old (weighing 15–19 g)/12-week-old (weighing 22–27 g) C57BL/6J mice were purchased from Southern Medical University Laboratory Animal Center. The animals were kept in the Animal Experiment Center of Nanfang Hospital, Southern Medical University on a 12-hour light-dark cycle, and had free access to food and water. The animal experiments complied with the National Institutes of Health Guide for the Care and Use of Laboratory Animals. All animal studies were approved by the Animal Use and Care Ethics Committee of Nanfang Hospital, Southern Medical University.

Animal models and treatments

IU1 and ETO was purchased from MedChemExpress (MCE, Shanghai, China). D-gal was obtained from Sigma (St. Louis, MO, USA). To confirm whether IU1 could ameliorate ETO-induced DNA damage in mouse granulosa cells in vivo, 6-week-old female C57BL/6J mice were randomly divided into 4 groups with 6 mice in each group. For the ETO group, mice were intraperitoneally injected with an equal volume of vehicle once a day for 14 days followed by an intraperitoneal injection of ETO (10 μg/g). Samples were collected 48 h after ETO injection. For the IU1 group, mice were intraperitoneally injected with IU1 40 mg/kg once a day for 14 days,

followed by an intraperitoneal injection of vehicle. Samples were collected 48 h after vehicle injection. For the IU1+ETO group, mice were intraperitoneally injected with IU1 40 mg/kg [21–23] once a day for 14 days followed by an intraperitoneal injection of ETO (10 μg/g). Samples were collected 48 h after ETO injection. The vehicle group received vehicle injections only.

To verify whether IU1 could improve ovarian function in the D-gal-induced POI mouse model, 12-week-old female C57BL/6J mice were randomly divided into 4 groups with 12 mice in each group. For the D-gal group, mice were intraperitoneally injected with vehicle and subcutaneously injected with D-gal (200 mg/kg) daily. For the IU1 group, mice were intraperitoneally injected with IU1 (40 mg/kg) and subcutaneously injected with vehicle daily. For the IU1+D-gal group, mice were intraperitoneally injected with 40 mg/kg IU1 and subcutaneously injected with 200 mg/kg D-gal daily. For the vehicle group, all injectable fluids were vehicle. After 6 weeks of continuous intervention, serum and ovaries were collected from the mice for subsequent experiments.

SA-β-galactosidase staining of cultured cells and frozen tissue sections

All staining procedures were performed according to the SA-β-galactosidase (SA-β-gal) staining kit manufacturer's instructions (Beyotime). Specifically, KGN cells were washed with PBS once and fixed in SA-β-gal staining fixative solution at room temperature for 15 min. Then, the cells were washed once with PBS. Staining solution A (10 μL), staining solution B (10 μL), staining solution C (930 μL) and X-Gal solution (10 μL) were mixed and adjusted to pH 6.5 before use. Subsequently, mixed staining solution was added to each well and incubated at 37 °C overnight, and the plate was sealed with plastic wrap to prevent evaporation. Images were scanned under an Olympus LX73 microscope (Olympus, Tokyo, Japan).

Frozen ovarian tissue sections were first rewarmed to room temperature for 10 min and fixed in SA-β-gal staining fixative solution for 15 min. The sections were then soaked in PBS 3 times for 5 min each. The mixed staining solution was prepared as described above. Each section was added to 500 μL staining solution, covered with sealing film to prevent evaporation and incubated in a wet box at 37 °C overnight. Afterward, the sections were immersed in PBS for 5 min and sealed with sealing solution. Finally, the images were scanned under a BX63 microscope (Olympus).

Enzyme-linked immunosorbent assay (ELISA) assay

Blood samples were obtained from model mice by removing their eyeballs after isoflurane gas anesthesia. Then, serum was isolated by centrifugation at 5000 rpm for 20 min after standing at room temperature for 2 h. Serum levels of FSH, AMH and E2 were measured by a Mouse FSH ELISA Kit (mlbio, Shanghai, China), Mouse AMH ELISA Kit (mlbio), and Mouse estradiol ELISA Kit (mlbio) according to the manufacturer's instructions.

Hematoxylin-eosin staining (HE)

Ovaries were fixed in 4% paraformaldehyde for 24 h, dehydrated in ethanol, embedded in paraffin and then cut into 4 μm sections. The sections were deparaffinized in xylene, rehydrated in a graded series of alcohols, stained with hematoxylin (Leagene, Beijing, China) for 3 min, immersed in 1% hydrochloric alcohol (Leagene) for 3 s and then immersed in deionized water to convert the hematoxylin to a dark blue color. Next, sections were stained with eosin (Leagene) for 30 s. After the sections were dried, neutral gel resin was used to seal the sections. The numbers of primordial follicles, primary follicles, secondary follicles, antral follicles, atresia follicles, and corpus luteum were estimated by counting every fifth section, and twenty sections from each ovary were counted.

Immunohistochemistry (IHC)

After deparaffinization, Tris-EDTA solution (pH=9.0, Servicebio) or citrate buffer (pH=6.0, Servicebio) was used for antigen repair, and the sections were soaked for 15 min in 3% hydrogen peroxide protected from light. After sealing with 5% goat serum for 30 min, the primary antibody was applied and incubated overnight at 4 °C. Then, the sections were washed 3 times with PBS and incubated with HRP-conjugated secondary antibody at room temperature for 1 h. Next, sections were stained with DAB working solution (Gene Tech, Shanghai, China, buffer A: buffer B solution=100:3) until yellow particles settled, and the reaction was terminated by rinsing with PBS. Subsequently, the sections were stained with hematoxylin for 20 s, immersed in 1% hydrochloric alcohol for 3 s, and immersed in deionized water to convert the hematoxylin to a dark blue color. After drying, the sections were sealed with neutral gel resin and photographed under a BX63 microscope (Olympus). When fluorescent secondary antibodies were used, the sections were incubated with the corresponding fluorescent secondary antibodies in a wet box at room temperature for 1 h and sealed with mounting medium with DAPI (Abcam). Subsequently, images were scanned under an Imager D2 (Zeiss) ortho-fluorescence microscope.

TdT-mediated dUTP nick end labeling (TUNEL staining)

The Fluorescein (FITC) TUNEL Cell Apoptosis Detection Kit (Servicebio) was used according to the manufacturer's instructions. Briefly, after the sections were deparaffinized, proteinase K was added to the sections and incubated for 20 min at 37 °C. After washing 3 times

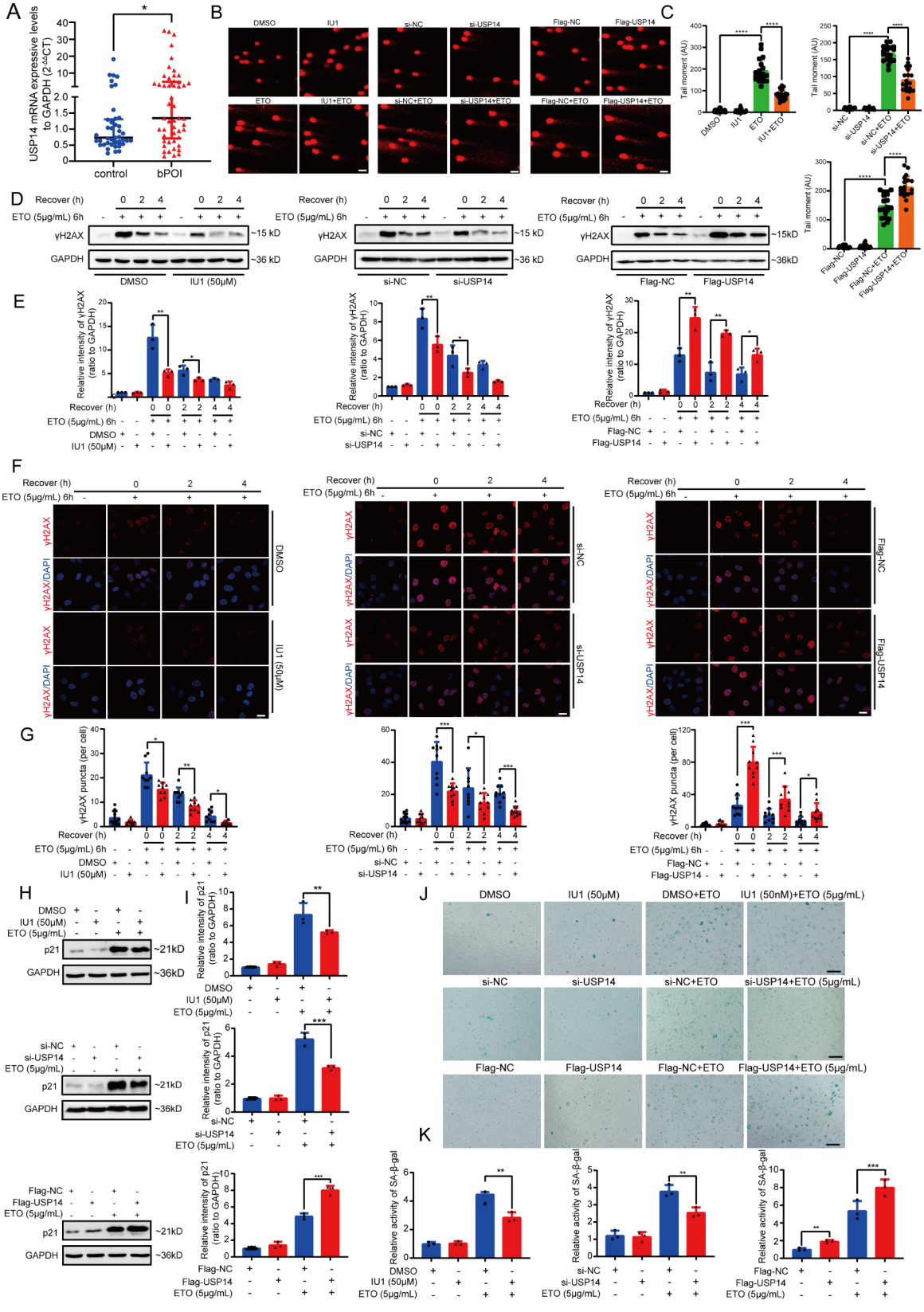

Fig. 1 (See legend on next page.)

(See figure on previous page.)

Fig. 1 USP14 affects DNA damage repair and aggravates the senescence of KGN cells. A The mRNA expression levels of USP14 in granulosa cells from bPOI and control patients were tested by qRT–PCR. Gene expression was normalized relative to GAPDH (mean ± SD). **B**, **C** Comet assay of KGN cells stimulated with 5 μg/mL ETO for 6 h with or without 24 h pretreatment with 50 μM IU1, transfected with si-NC or si-USP14, and overexpressing Flag-NC or Flag-USP14 before ETO induction (bar = 50 μm). **D**, **E** Western blot of γH2AX in KGN cells at 0 h, 2 h and 4 h after ETO induction for 6 h with or without pretreatment with 50 μM IU1 for 24 h, transfected with si-NC or si-USP14, and overexpressing Flag-NC or Flag-USP14. **F**, **G** Immunofluorescence assay of γH2AX in KGN cells at 0 h, 2 h and 4 h after ETO induction for 6 h with or without pretreatment with 50 μM IU1 for 24 h, transfected with si-NC or si-USP14, and overexpressing Flag-NC or Flag-USP14 (bar = 10 μm). **H**, **I** Western blot analysis of p21 in KGN cells after ETO induction for 12 h with or without pretreatment with 50 μM IU1 for 24 h, transfected with si-NC or si-USP14, and overexpressing Flag-NC or Flag-USP14. **J**, **K** SA-β-Gal staining of KGN cells after ETO induction for 12 h with or without pretreatment with 50 μM IU1 for 24 h, transfection with si-NC or si-USP14, or Flag-NC or Flag-USP14 overexpression. (bar = 50 μm). All the data are presented as the means ± SDs of at least three independent experiments; *$P < 0.05$, **$P < 0.01$, ***$P < 0.001$, ****$P < 0.0001$

with PBS, each section was covered with 10 μL of 0.2% Triton-X 100 at room temperature for 20 min, followed by 10 μL of equilibration buffer at room temperature for 10 min. Then, the TdT incubation buffer was prepared according to the ratio of recombinant TdT enzyme: FITC-12-dUTP labeling mix: equilibration buffer = 1:5:50, and 10 μL of mixed buffer was added to each section and incubated for 1 h at 37 °C in the dark. Finally, sections were sealed with mounting medium with DAPI (Abcam), and images were scanned under an Imager D2 (Zeiss) ortho-fluorescence microscope.

Statistical analysis

All experimental data are represented as the mean ± SD of at least three independent experiments. *P* values were calculated using GraphPad Prism Software. Unpaired two-sided Student's t test was used to compare the differences between two groups, while one-way ANOVA was used for multiple groups. All significant differences are shown as *$P < 0.05$, **$P < 0.01$, ***$P < 0.001$, and ****$P < 0.0001$.

Results

The USP14 mRNA expression level is significantly increased in the hLGCs of bPOI patients

In our study, hLGCs from 50 bPOI patients and 41 control patients were collected. The clinical data of the two groups are shown in Supplementary Tables 1, and there were no significant differences in age, body mass index (BMI), or basal luteinizing hormone (LH) levels between the two groups. In the bPOI group, AMH, estradiol levels and the AFC were lower than those in the control group, while basal FSH levels were higher than those in the control group ($P < 0.001$). The USP14 mRNA expression level in the control group and bPOI group hLGCs was measured by qRT−PCR. Compared with that in the control group, the expression level of USP14 was significantly increased in the bPOI group refer to GAPDH (Fig. 1A). Furthermore, we analyzed the correlation between the mRNA expression level of USP14 in hLGCs and the clinical data on patient age, ovarian reserve function (AFC, AMH, basal FSH), number of retrieved oocytes, and oocyte quality (oocyte maturation rate, normal fertilization rate, available embryo rate) by Spearman correlation analysis. The results showed that there was a negative correlation between the expression level of USP14 and the AFC as well as the number of retrieved oocytes but no significant correlation with other clinical information (Supplementary Table 2), indicating that USP14 may play a negative role in the ovarian reserve.

USP14 affects the DDR function of granulosa cells

As USP14 has been reported to regulate DDR in prostate and lung cancers, the effect of USP14 on DDR function in granulosa cells was first investigated by using KGN cells as an in vitro model. KGN cells were stimulated with 5 μg/mL ETO for 6 h to induce cellular DNA damage, and comet assays were performed to evaluate DNA damage. As expected, the level of DNA damage in KGN cells was significantly increased after ETO induction, and pretreatment with 50 μM IU1 [19, 21], a USP14-specific allosteric inhibitor, for 24 h significantly reduced ETO-induced DNA damage in KGN cells (Supplementary Fig. 1A, Fig. 1B and 1C). USP14 was also inhibited by transfection with siRNA-USP14 (si-USP14, Supplementary Fig. 1B) in KGN cells, and similar to the effect of IU1 treatment, ETO-induced DNA damage was decreased in the si-USP14 group (Fig. 1B and C). KGN cell lines overexpressing USP14 were infected with lentivirus (Supplementary Fig. 1C). The overexpression of USP14 significantly enhanced ETO-induced DNA damage in KGN cells (Fig. 1B and C). To further investigate the regulatory effect of USP14 on the DDR function of KGN cells, the γ-H2AX protein expression level and the number of γ-H2AX foci were examined in cells treated with 5 μg/mL ETO for 6 h, and 2 h and 4 h after ETO was removed. The results showed that the protein expression level of γH2AX significantly increased after 6 h of ETO induction in KGN cells and gradually decreased at 2 h and 4 h after the removal of ETO (Fig. 1D-E). Compared with those in the DMSO group and si-NC group, ETO-induced γH2AX protein expression was downregulated after 24 h of pretreatment with 50 μM IU1 and si-USP14, and was also reduced after 2 h of DDR, indicating that IU1 and si-USP14 increased the resistance of KGN cells to ETO-induced DNA damage and enhanced cellular DDR function (Fig. 1D-E). In USP14-overexpressing cells, the protein expression of γH2AX was significantly

increased after ETO stimulation as well as 2 h and 4 h after ETO removal, suggesting that overexpression of USP14 impaired the DDR of KGN cells (Fig. 1D-E). Similarly, in KGN cells, the number of γ-H2AX foci significantly increased after 6 h of ETO induction and gradually decreased 2 h and 4 h after ETO removal (Fig. 1F-G). Compared with DMSO and si-NC treatment, pretreatment with 50 μM IU1 and si-USP14 significantly reduced the number of γ-H2AX foci, whereas overexpression of USP14 significantly increased the number of γ-H2AX foci (Fig. 1F-G). These data indicated that USP14 was involved in the regulation of DDR function in KGN cells. Specifically, inhibition of USP14 promoted DDR, while overexpression of USP14 inhibited DDR.

USP14 aggravates DNA damage-induced senescence in granulosa cells

As persistent DDR dysfunction induces cell senescence [10], the cellular senescence of KGN cells was tested after treatment with 5 μg/mL ETO for 12 h. The protein expression level of p21, a marker of cellular senescence, was significantly increased after ETO stimulation. In addition, 24 h of pretreatment with 50 μM IU1 and transfection with si-USP14 significantly downregulated ETO-induced p21 expression, while overexpression of USP14 significantly upregulated p21 expression (Fig. 1H-I). The activity of senescence-associated SA-β-Gal was further examined [24], and SA-β-Gal activity significantly increased after 12 h of ETO stimulation in KGN cells, and pretreatment with 50 μM IU1 for 24 h or transfection with si-USP14 significantly inhibited ETO-induced SA-β-Gal activity (Fig. 1J-K). In addition, overexpression of USP14 substantially increased ETO-induced SA-β-Gal activity (Fig. 1J-K). The above results suggested that inhibition of USP14 suppressed DNA damage-induced cellular senescence, while overexpression of USP14 played a promotive role.

USP14 affects the NHEJ pathway in granulosa cells

Previous studies have shown that USP14 suppressed DDR primarily through the regulation of the NHEJ pathway [18], so we examined the expression level of 53BP1 protein and the number of 53BP1 foci, as 53BP1 is known as a key factor in the NHEJ pathway. When KGN cells were pretreated with 50 μM IU1 or transfected with si-USP14, the protein expression level of 53BP1 and the number of 53BP1 foci significantly increased after 2 h and 4 h of DDR (Fig. 2A-D). Conversely, overexpression of USP14 inhibited the protein expression of 53BP1 and decreased the number of 53BP1 foci (Fig. 2A-D). Given that the phosphorylation of DNA-PKcs is essential for the activation of the DNA-PK holoenzyme and promotes the subsequent NHEJ pathway [25], the expression levels of phosphorylated DNA-PKcs (p-DNA-PKcs) were measured at 2 h and 4 h after ETO induction. Consistent with those of 53BP1, p-DNA-PKcs expression in KGN cells showed the same trend after pretreatment with 50 μM IU1, si-USP14 transfection or overexpression of USP14 (Fig. 2A-D). These results suggest that USP14 may be involved in the DDR function of KGN cells by regulating the NHEJ pathway.

USP14 regulated the DDR function of granulosa cells via RNF168, Ku70, and DDB1

RNF168 and Ku70 are downstream molecules of USP14 that regulate the NHEJ pathway [16, 17], and USP14 may act by directly affecting their protein expression levels and antagonizing the ubiquitination of downstream molecules. Therefore, the protein expression levels of RNF168 and Ku70 were tested after ETO induction. Pretreatment with 50 μM IU1 for 24 h and transfection with si-USP14 significantly increased the protein expression levels of RNF168 and Ku70 after 2 h and 4 h of DDR compared with those in the DMSO and si-NC group (Fig. 3A-B), and the overexpression of USP14 significantly inhibited the expression levels of Ku70 at 2 h and 4 h after DDR and the expression levels of RNF168 at 2 h (Fig. 3A-B).

RNF168 is a key E3 ubiquitin ligase that catalyzes K13/K15 ubiquitination in H2A [26]. Therefore, to further verify whether USP14 can affect the function of RNF168 in KGN cells, the monoubiquitination of H2AX protein was examined after ETO induction. The results showed that pretreatment with 50 μM IU1 and transfection with si-USP14 significantly promoted the monoubiquitination of H2AX after 2 h and 4 h of DDR (Fig. 3C), while overexpression of USP14 decreased the monoubiquitination of H2AX (Fig. 3C). Immunofluorescence staining also revealed that the colocalization of γH2AX with ubiquitin molecules was reduced after 6 h of ETO stimulation in USP14-overexpressing KGN cells (Fig. 3D).

To further explore whether there are other important downstream molecules involved in the regulation of DDR by USP14 in granulosa cells, we searched the literature and found that Liu B et al. performed a co-IP proteomic assay in 293T cells with Flag-USP14 overexpression and sequenced the upregulated ubiquitination sites in HeLa cells with USP14 knockdown. Through intersection of two sets of sequencing data, a DDR-related protein, DDB1, was shown to bind with USP14, and USP14 may decrease its ubiquitination level [27]. Hence, we speculated that DDB1 may also be a downstream target of USP14 in the regulation of DDR in KGN cells.

DDB1 is thought to be a key molecule in nucleotide excision repair (NER) because of its important role in the recognition of ultraviolet (UV)-induced base damage. In recent years, this molecule has been found to play an important role in other DDR processes [28]. We

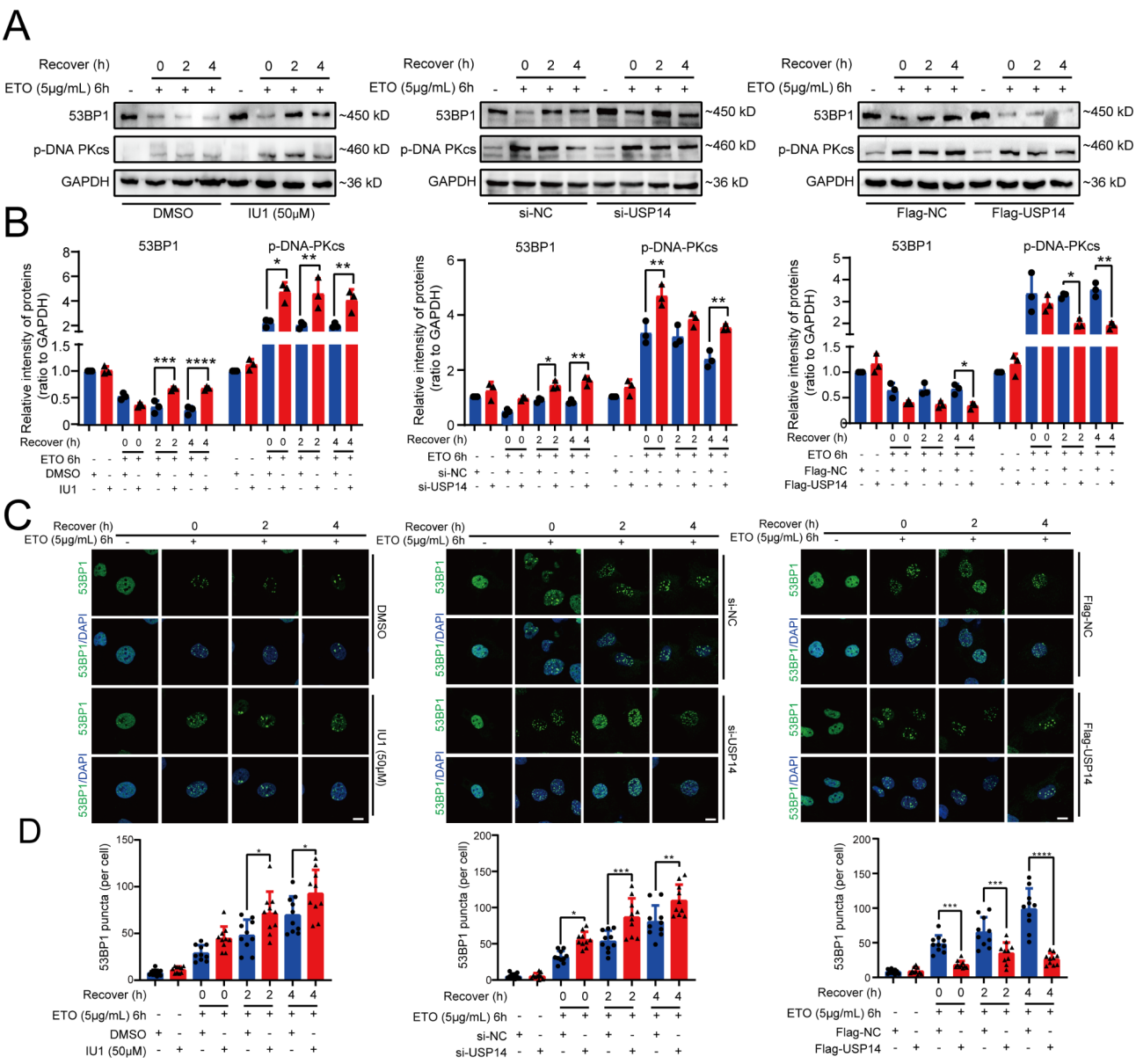

Fig. 2 USP14 impairs the NHEJ pathway in KGN cells. A, **B** Western blot analysis of 53BP1 and p-DNA-PKcs in KGN cells at 0 h, 2 h and 4 h after ETO induction for 6 h with or without pretreatment with 50 μM IU1 for 24 h, transfection with si-NC or si-USP14, and Flag-NC or Flag-USP14 overexpression. **C**, **D** Immunofluorescence assay of 53BP1 in KGN cells at 0 h, 2 h and 4 h after ETO induction for 6 h with or without pretreatment with 50 μM IU1 for 24 h, transfection with si-NC or si-USP14, and overexpression of Flag-NC or Flag-USP14. (bar = 10 μm). All the data are presented as the means ± SDs of at least three independent experiments; **P* < 0.05, ***P* < 0.01, ****P* < 0.001, ****P<0.0001

first assessed whether USP14 affects DDB1 expression in KGN cells. Compared with DMSO treatment, 24 h of pretreatment with 50 μM IU1 significantly increased the protein expression levels of DDB1 after 2 h and 4 h of DDR (Fig. 3A-B), and the overexpression of USP14 significantly inhibited the expression levels of DDB1 after 2 h and 4 h (Fig. 3A-B).

A co-IP assay was performed to explore whether USP14 can interact with DDB1. The Flag-USP14 overexpression vector and His-DDB1 overexpression vector were cotransfected into HEK293T cells, Flag-tagged USP14 was detected by IP with a His antibody (Fig. 3E), and His-tagged DDB1 was detected by IP with a Flag antibody (Fig. 3F), suggesting that USP14 can interact with DDB1. Next, to verify whether USP14 mediates the deubiquitination of DDB1, we cotransfected HEK293T cells with the HA-Ub overexpression vector and His-DDB1 overexpression vector. After treatment with the proteasome inhibitor MG132 for 10 h, we incubated the cells with the His antibody and detected the Ub signal. The results showed that the ubiquitination level of DDB1 decreased after treatment with 50 μM IU1 for 24 h (Fig. 3G) and

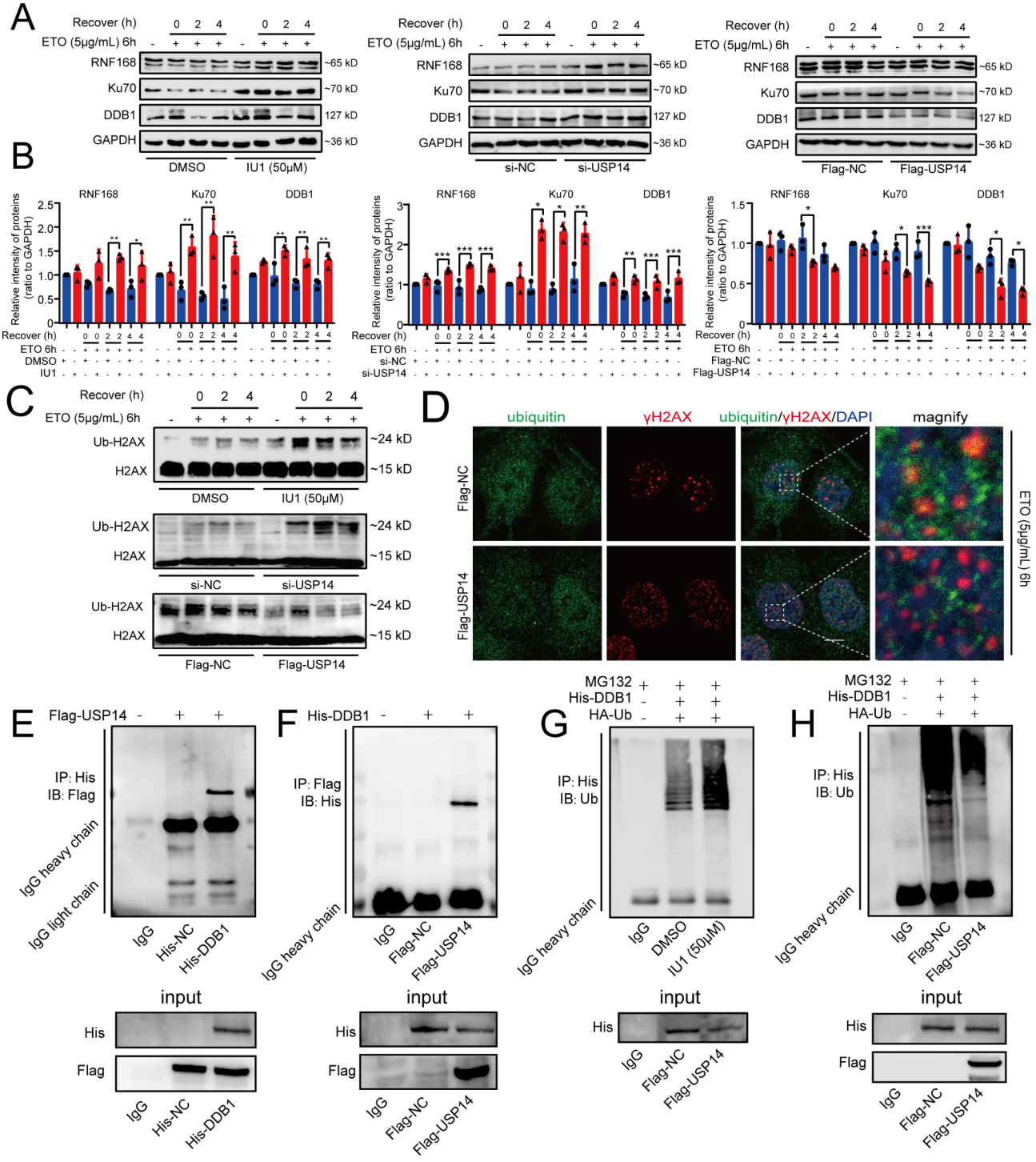

Fig. 3 USP14 regulates the expression of RNF168, Ku70, DDB1 and ubiquitination of DDB1. A, **B** Western blot analysis of RNF168, Ku70 and DDB1 in KGN cells at 0 h, 2 h and 4 h after ETO induction for 6 h with or without pretreatment with 50 μM IU1 for 24 h, transfection with si-NC or si-USP14, and overexpression of Flag-NC or Flag-USP14. **C** Western blot analysis of H2AX monoubiquitination in KGN cells at 0 h, 2 h and 4 h after ETO induction for 6 h with or without pretreatment with 50 μM IU1 for 24 h, transfection with si-NC or si-USP14, and overexpression of Flag-NC or Flag-USP14. **D** Immunofluorescence assay showing the colocalization of γH2AX and ubiquitin in KGN cells overexpressing USP14 after stimulation with 5 μg/mL ETO for 6 h (scale bar = 5 μm). **E** Co-IP assay of Flag expression in HEK 293T cells overexpressing Flag-USP14 and His-DDB1 by IP with the His antibody. **F** Co-IP assay of His expression in HEK 293T cells overexpressing Flag-USP14 and His-DDB1 by IP with an anti-Flag antibody. **G** Co-IP assay of Ub expression in HEK 293T cells overexpressing His-DDB1 and HA-Ub with or without pretreatment with 50 μM IU1 for 24 h by IP with the His antibody. **H** Co-IP assay of Ub expression in HEK 293T cells overexpressing Flag-USP14, His-DDB1 and HA-Ub by IP with the His antibody. All data are presented as the means ± SDs of at least three independent experiments; *$P < 0.05$, **$P < 0.01$, ***$P < 0.001$

increased after overexpression of USP14 (Fig. 3H), suggesting that USP14 promoted the deubiquitination of DDB1.

USP14 regulates the DDR function of granulosa cells in vivo

To determine whether USP14 can also affect the DDR function of granulosa cells in vivo, we intraperitoneally administered 40 mg/kg IU1 daily for 14 days, followed by intraperitoneal injection of 10 μg/g ETO to induce DNA damage, and then collected the samples 48 h after ETO injection. The percentage of γH2AX-positive granulosa cells in the ovaries of the ETO group was significantly greater than that in ovaries of the control group, and the percentage of γH2AX-positive granulosa cells in the ovaries of the IU1+ETO group was significantly lower than that in the ovaries of the ETO group (supplementary Fig. 2A). Since poly (ADP-ribose) polymerase (PARP) is a key signal for intracellular recognition of DNA single-strand breaks and the initiation of DDR reactions, and since cleaved-PARP is the active form of PARP [29], we also determined the percentage of cleaved-PARP-positive granulosa cells in the ovaries of mice in different groups. Similar to the γH2AX results, the proportion of cleaved PARP-positive granulosa cells in the ovaries of the ETO group was significantly greater than that in the ovaries of the control group, and IU1 treatment markedly inhibited this increase (Supplementary Fig. 2B).

IU1 alleviates D-gal-induced premature ovarian senescence

Next, we further verified whether IU1 could be used as a potential therapeutic agent for POI. Previous research has shown that the accumulation of D-gal in vivo has toxic effects on the ovary, and mice receiving subcutaneous injections of D-gal showed reduced follicle numbers, absence of mature follicles and increased follicular atresia similar to the characteristics of POI, suggesting that D-gal is an appropriate agent for inducing premature ovarian senescence [30]. Therefore, we used D-gal subcutaneous injection for POI modeling. We first performed IHC to determine the expression and localization of USP14 in the ovaries of different groups. The results showed that USP14 was widely expressed in ovarian granulosa cells, oocytes and stromal cells, and the expression level of USP14 was increased after D-gal stimulation. (Supplementary Fig. 3). The number of primordial follicles, secondary follicles, antral follicles, and corpus luteum were significantly reduced in the D-gal group compared with the control group, and the number of atretic follicles was significantly increased in the D-gal group (Fig. 4A, B). However, IU1 treatment greatly relieved these changes, resulting in a significant increase in the number of primordial follicles, antral follicles, and corpus luteum, accompanied by a significant decrease in atresia follicle numbers (Fig. 4A, B). The levels of serum AMH and estradiol were decreased and the levels of FSH were increased in the D-gal group compared with the control group, but the administration of IU1 significantly abrogated these changes (Fig. 4C-E).

IU1 treatment significantly ameliorated D-gal-induced DNA damage and cell senescence of granulosa cells in vivo

Firstly, we examined the DNA breakage of granulosa cells using a TUNEL assay. The results showed that the proportion of TUNEL-positive granulosa cells in the D-gal group was significantly increased compared to that in the control group but was significantly decreased in the IU1+D-gal group compared to the D-gal group (Fig. 5A). Then, immunofluorescence staining was used to determine the proportion of γH2AX-positive and cleaved PARP-positive granulosa cells in the ovaries. The results showed the same trend; the proportions of γH2AX-positive and cleaved-PARP-positive ovarian granulosa cells in the D-gal group were significantly increased compared with those in the control group and significantly decreased after IU1 treatment (Fig. 5B, C).

We have demonstrated that IU1 significantly ameliorates DNA damage-induced cell senescence in vitro. Furthermore, whether IU1 could improve granulosa cell senescence induced by D-gal in vivo was confirmed. We examined SA-β-Gal activity in ovarian tissues and found that the largest area of positive SA-β-Gal staining was found in the D-gal group, indicating that the cell senescence degree of this group was higher than that of the other groups, while IU1 reduced D-gal-induced SA-β-Gal activity (Fig. 6A). The p21 staining results showed that the proportion in the ovaries of the D-gal group was increased; however, the proportion of p21-positive granulosa cells was significantly reduced in the IU1+D-gal group (Fig. 6B). Furthermore, previous studies have reported that an elevated fibrosis level of the ovarian stroma is also an important indicator of ovarian senescence, so we performed Masson staining to detect fibrosis in the ovarian tissue and showed that the area of fibrosis was increased in the D-gal group compared to the control group and that IU1 could significantly alleviate D-gal-induced fibrosis (Fig. 6C).

Proliferating cell nuclear antigen (PCNA) is an important marker of cell proliferation [31]. As previously mentioned, an important feature of cell senescence is proliferative arrest, and the expression level of β-Gal is also an important indicator of cell senescence [32]. Therefore, we applied IHC to determine the proportions of PCNA- and β-Gal-positive cells in ovarian granulosa cells. Compared with the control group, the D-gal-treated group exhibited a significant decrease in the proportion of PCNA-positive granulosa cells and an

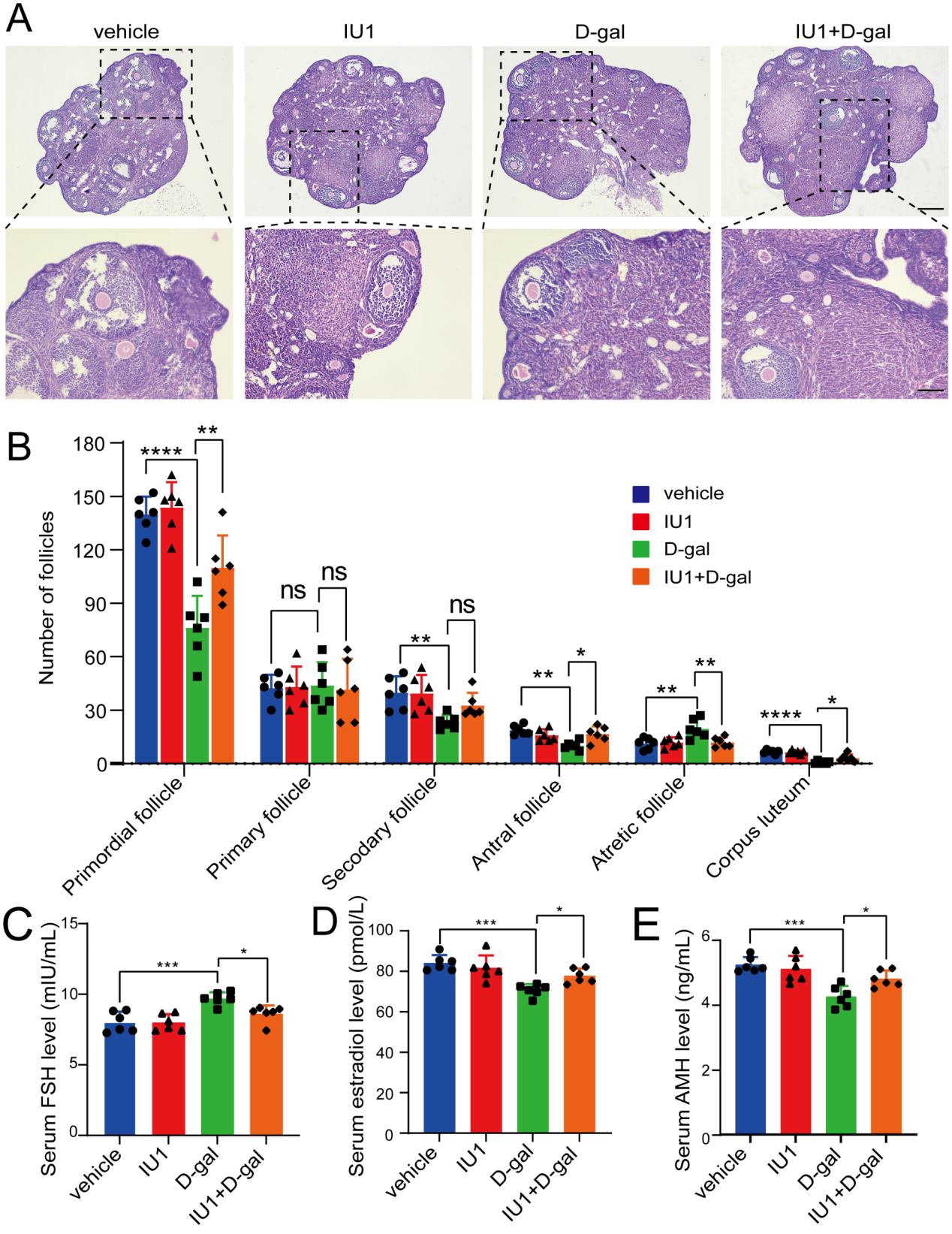

Fig. 4 Treatment with IU1 ameliorates the decreased ovary reserve in D-gal-induced POI model mice. A Representative HE staining of mouse ovary sections from different groups (bar = 500 μm, 100 μm; $n = 6$). **B** Counts of primordial follicles, primary follicles, secondary follicles, antral follicles, atretic follicles and corpus luteum in every mouse ovary ($n = 6$). **C-E** ELISAs of serum FSH, estradiol and AMH levels in mice from each group ($n = 6$). All data are presented as the means ± SDs; $^{*}P < 0.05$, $^{**}P < 0.01$, $^{***}P < 0.001$, $^{****}P < 0.0001$

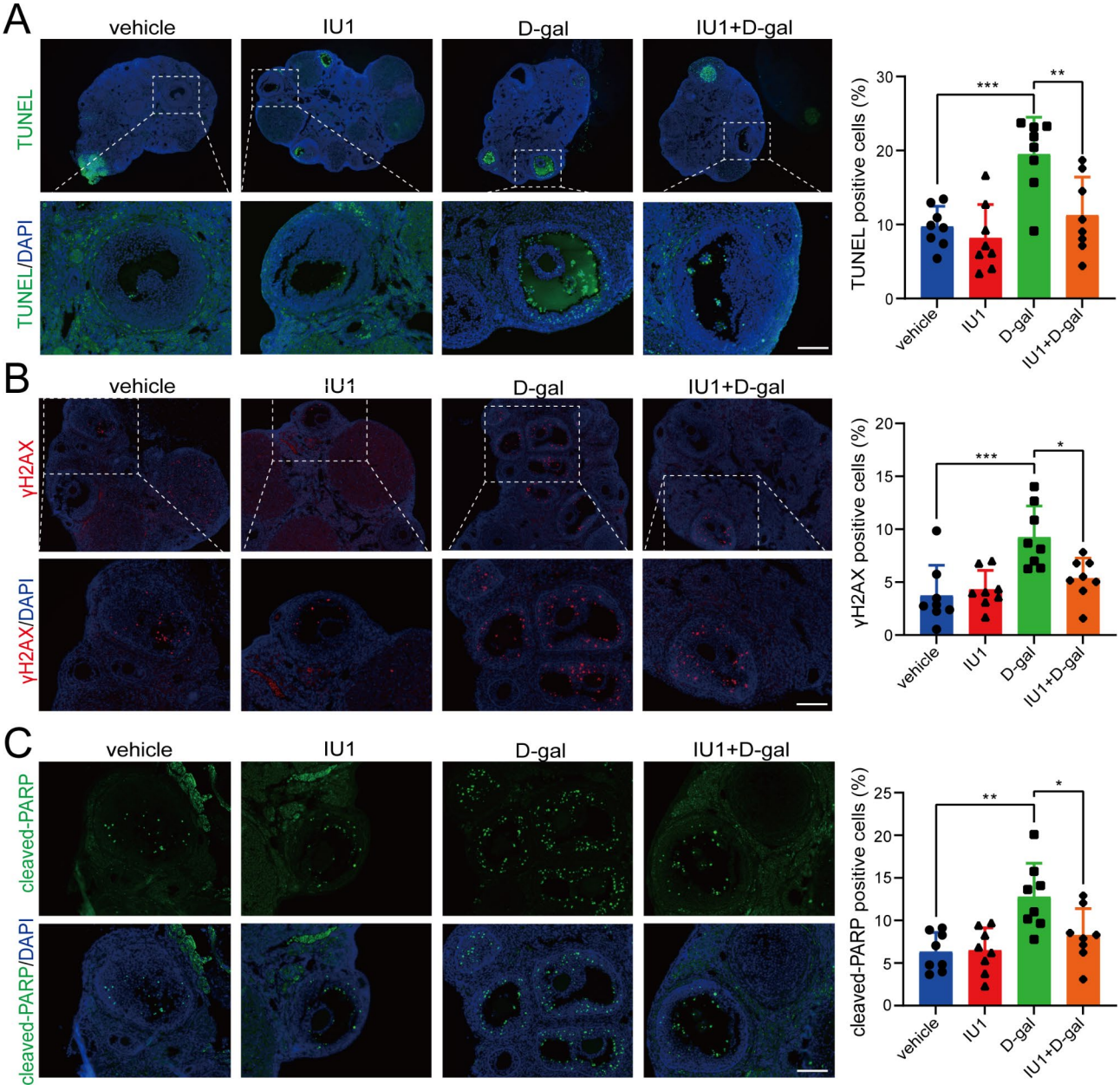

Fig. 5 IU1 alleviates D-gal-induced DNA damage in mouse ovarian granulosa cells. A TUNEL staining of DNA damage in mouse ovarian granulosa cells. (bar = 100 μm; $n = 6$) **B** Immunofluorescence assay of γH2AX in mouse ovarian granulosa cells (bar = 100 μm; $n = 6$). **C** Immunofluorescence assay of and cleaved PARP in mouse ovarian granulosa cells (bar = 100 μm; $n = 6$). All data are presented as the means ± SDs; $^{*}P < 0.05$, $^{**}P < 0.01$, $^{***}P < 0.001$

increase in the proportion of β-Gal-positive cells; however, the application of IU1 reversed the changes caused by D-gal (Fig. 6D-E).

The western blot results also showed that in the D-gal group, β-gal and γH2AX expression levels were higher and PCNA expression levels were lower than those in the control group. Moreover, β-gal and γH2AX expression was downregulated and PCNA expression was upregulated in the IU1 + D-gal group compared to the D-gal group (Fig. 6F). Based on the above results, intraperitoneal IU1 injection significantly improved the DNA damage and cell senescence phenotype of granulosa cells in POI model mice.

IU1 treatment promotes the NHEJ pathway in granulosa cells in vivo

We verified in vitro that IU1 may primarily increases NHEJ pathway activity in cells by affecting the expression and function of RNF168, Ku70, and DDB1, thereby promoting the DDR of granulosa cells. Therefore, we also examined the expression levels of 53BP1, RNF168, Ku70 and DDB1 in mouse ovarian granulosa cells. The

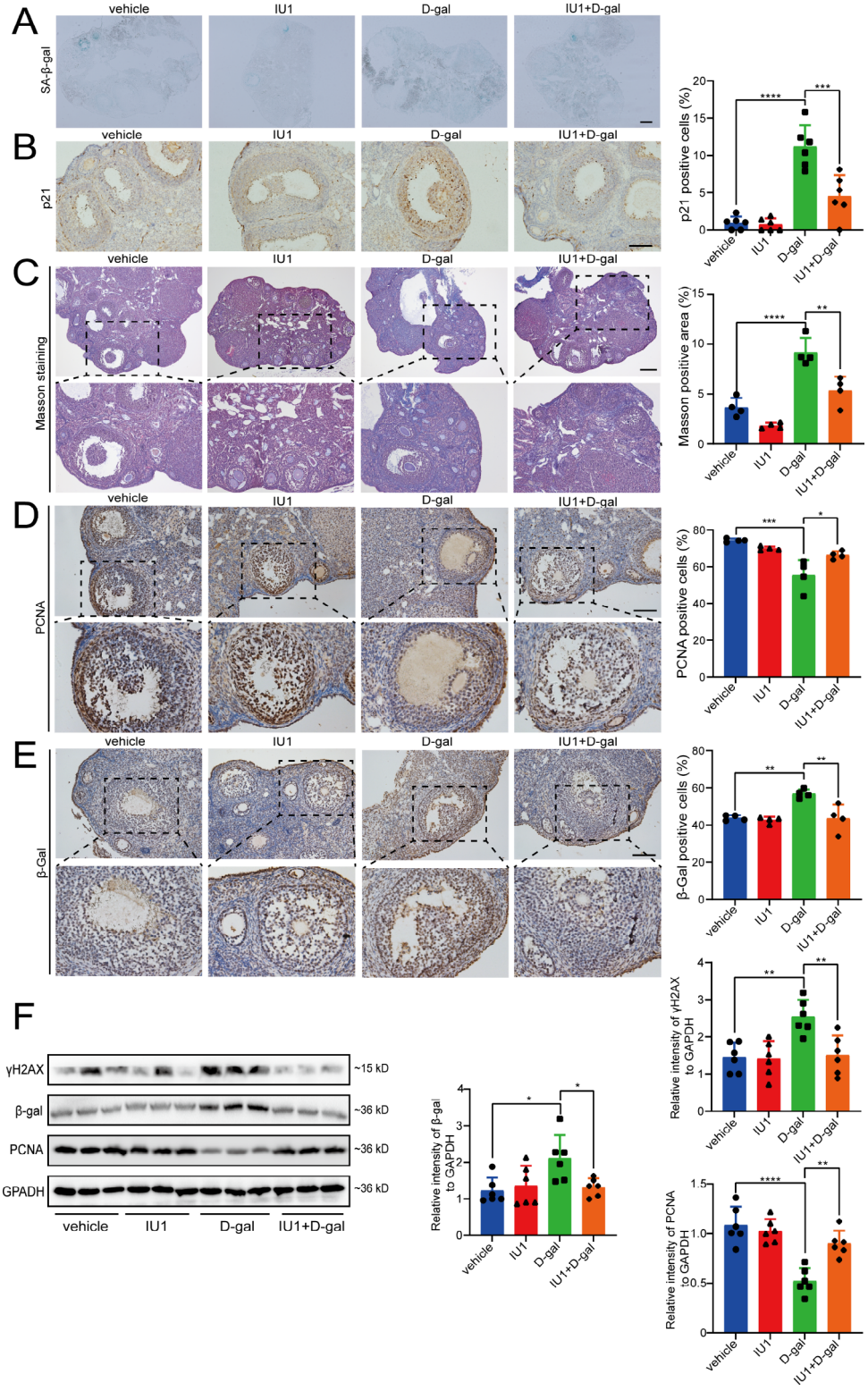

Fig. 6 IU1 improves D-gal-induced ovarian senescence in mice. A SA-β-gal staining of mouse ovary sections from different groups. (bar = 100 μm; $n = 4$) **B** IHC assay of p21-positive granulosa cells in mouse ovarian granulosa cells. (bar = 100 μm; $n = 6$) **C** Masson staining for ovarian fibrosis in mouse ovaries (bar = 100 μm; $n = 4$) **D** IHC assay of PCNA in mouse ovarian granulosa cells. (bar = 100 μm; $n = 4$) **E** IHC assay of β-gal in mouse ovarian granulosa cells. (bar = 100 μm; $n = 4$) **F** Western blot analysis of γH2AX, β-gal, and PCNA in mouse ovaries from different groups. GAPDH was used as a loading control ($n = 6$). All data are presented as the means ± SDs, $^{*}P < 0.05$, $^{**}P < 0.01$, $^{***}P < 0.001$, $^{****}P < 0.0001$.

IHC results showed that the percentages of 53BP1- and DDB1-positive cells in the IU1+D-gal group were significantly higher than those in the D-gal group (Fig. 7A, B). In accordance with the IHC results, the protein expression levels tested by Western blotting showed the same trend; RNF168, Ku70 and DDB1 were significantly upregulated in the IU1+D-gal group compared with the D-gal group (Fig. 7C). All the data indicated that IU1 also upregulates the protein expression of RNF168, Ku70 and DDB1 in vivo and promotes DDR through the NHEJ pathway in granulosa cells (Fig. 8).

Discussion

Abnormal DDR function in granulosa cells may be one of the pathogenic mechanisms of POI [33]. USP14 is an important enzyme involved in the regulation of DDR-related protein ubiquitination modifications, but there is no report on whether USP14 is associated with the development of POI to date. This study demonstrated that high expression of USP14 in granulosa cells from patients with bPOI impaired DDR function and accelerated cellular senescence of granulosa cells, which was possibly mediated by its regulation of the expression and ubiquitination of RNF168, Ku70 and DDB1. Moreover, IU1, a

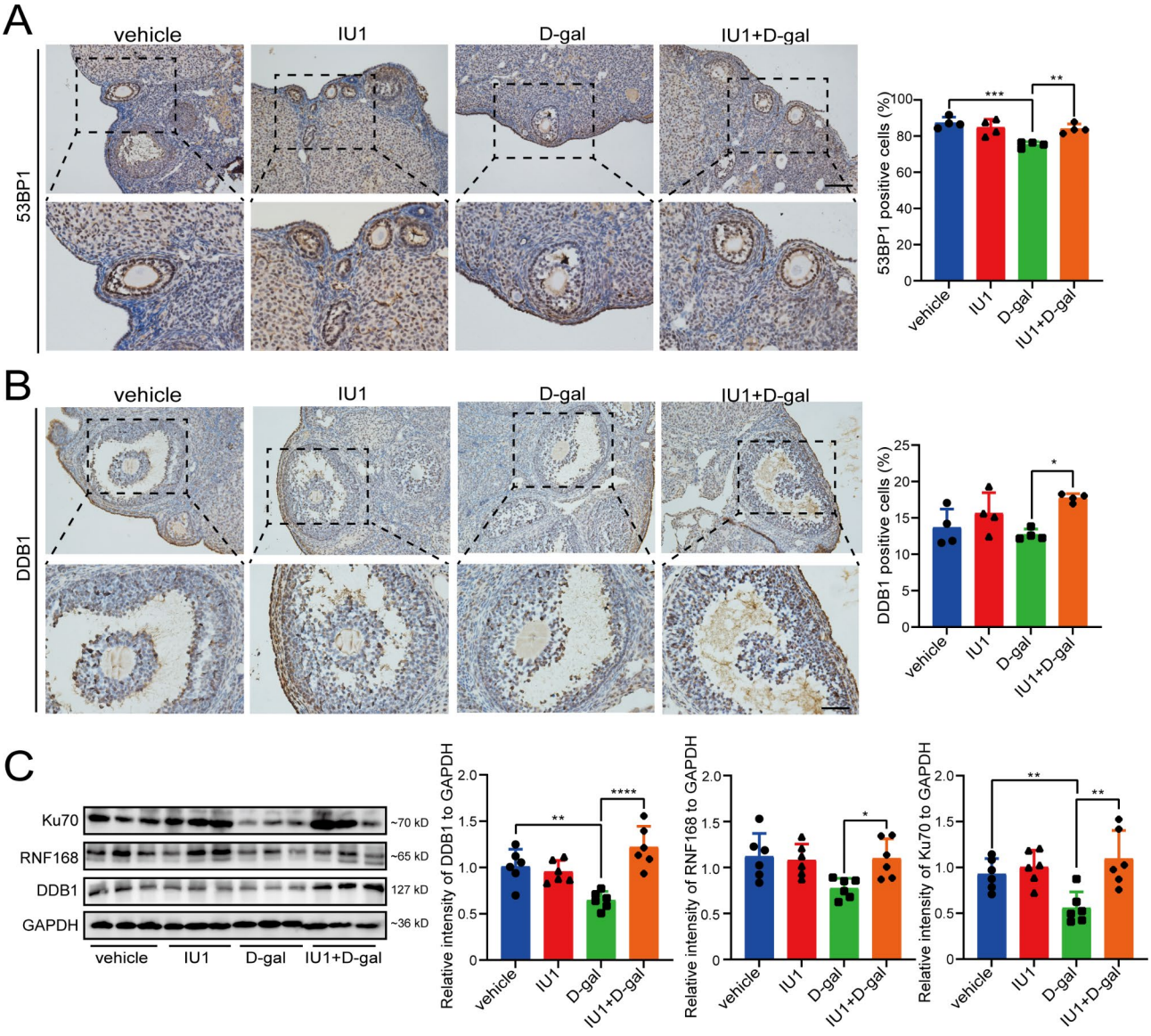

Fig. 7 IU1 affects the expression of 53BP1, Ku70, RNF168 and DDB1 in mouse ovaries. A IHC assay of 53BP1 in mouse ovarian granulosa cells. (bar = 100 μm; $n = 4$) **B** IHC assay of DDB1 in mouse ovarian granulosa cells. (bar = 50 μm; $n = 4$) **C** Western blot analysis of Ku70, RNF168 and DDB1 in mouse ovaries from different groups. GAPDH was used as a loading control ($n = 6$). All data are represented as the mean ± SD, $^{*}P < 0.05$, $^{**}P < 0.01$, $^{***}P < 0.001$, $^{****}P < 0.0001$

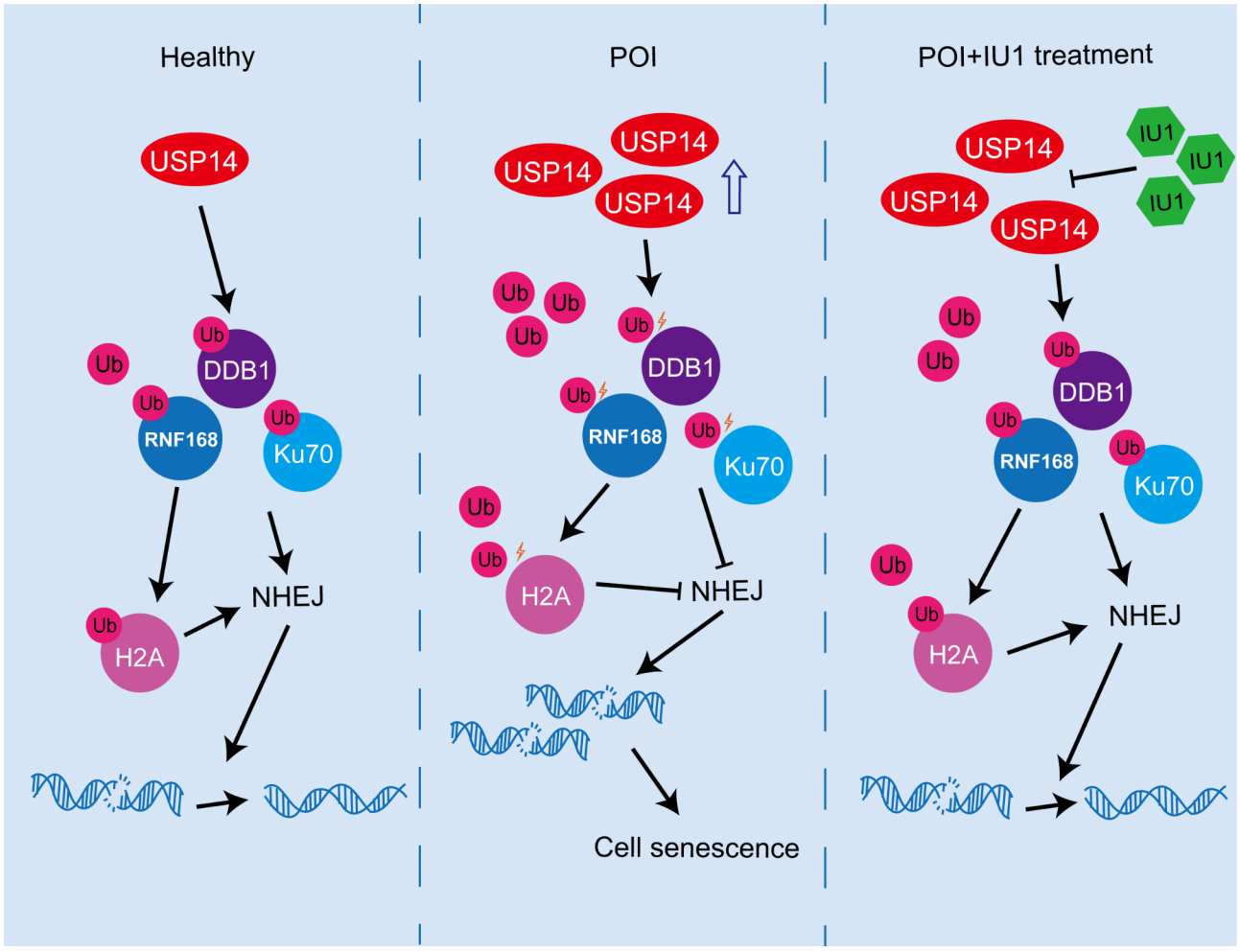

Fig. 8 Schematic illustration of the mechanism by which USP14 regulates DNA damage repair and cell senescence of granulosa cells in POI. In healthy granulosa cells, modest amounts of USP14 maintain the ubiquitination of RNF168, Ku70 and DDB1 thereby regulating the NHEJ pathway and leading to normal DDR. In granulosa cells with POI, the expression of USP14 was significantly upregulated, resulting in impaired DDR function and cellular senescence via decreases in the expression and ubiquitination of RNF168, Ku70 and DDB1. By targeted inhibition of USP14 using IU1, the dysfunction of granulosa cells was significantly reversed

specific inhibitor of USP14, significantly improved the phenotypes of D-gal-induced POI model mice.

USP14 contains two surface loops, BL1 and BL2. In free USP14, BL1 and BL2 block the binding pocket to prevent binding to the C-terminus of ubiquitin molecules. After USP14 binds to the 19 S of the proteasome, it undergoes a substantial conformational change, with BL1 and BL2 shifting to allow the C-terminus of the ubiquitin molecule to enter the binding site and catalyze the hydrolysis of the ubiquitin chain, thus acting as a deubiquitinating enzyme [34]. As ubiquitylation plays an important role in maintaining protein stability, regulating protein molecule interactions, and modulating enzyme activity, USP14 is involved in a variety of physiological processes and diseases by affecting the stability and function of many proteins [35–37]. For example, USP14 inhibits endoplasmic reticulum-associated protein degradation by binding to the inactivated IRE1 protein in the cytoplasm, thereby promoting virus replication and propagation. During the immune response, USP14 stabilizes the CXCR4 protein by mediating its deubiquitination and thereby promotes inflammatory cell chemotaxis [38]. Furthermore, USP14 was shown to activate the NF-κB pathway by promoting the degradation of IκB, resulting in inflammatory response activation [39]. Moreover, USP14 has been reported to be involved in the pathogenesis of neurodegenerative diseases, including Alzheimer's disease, Parkinson's disease, Huntington's disease and amyotrophic lateral sclerosis, which are characterized by the accumulation or aggregation of ubiquitinated proteins in the central nervous system. The deubiquitinase activity of USP14 leads to the impaired degradation of pathological proteins, thus contributing to the progression of these diseases [14]. In addition, USP14 can promote the

progression of several malignant cancers, such as breast cancer [40], colon cancer [19] and liver cancer [21], and some metabolic-related diseases, such as fatty liver disease [27] and diabetes [37].

However, few studies have focused on the function of USP14 in the ovary and its possible role in the pathogenesis of POI. It has been reported that USP14 expression was downregulated by approximately 75% in the ovaries of female homozygous ataxia mice, but female fertility was not affected. However, USP14 expression was downregulated by approximately 50% in the testes of male mice with homozygous ataxia, leading to a marked reduction in testicular volume, increased abnormal sperm count, and male sterility phenotype, suggesting that USP14 plays an important role in spermatogenesis [41]. In addition, Wang Y et al. reported that USP14 promotes the development of ovarian epithelial tumors [18]. Our study revealed that the upregulation of USP14 in granulosa cells is involved in POI pathogenesis, possibly by promoting granulosa cells' DNA damage and cellular senescence. Considering the complex and diverse effects of USP14 on cell function, it would be worthwhile to investigate whether USP14 can affect granulosa cell function through other molecular mechanisms. In our study, we only focused on the effect of USP14 in granulosa cells, and its effects on other cell types remains unclear. Therefore, further studies are needed to explore its effects on oocytes and stromal cells of ovary.

As USP14 is involved in the pathogenesis of many diseases, the therapeutic role of IU1, a small molecule inhibitor of USP14, has been widely studied. Shi D et al. reported that compared with anti-PD1 therapy alone, 40 mg/kg IU1 administered intraperitoneally daily in combination with anti-PD1 therapy significantly reduced subcutaneous colon tumor volume in mice [19]. Moreover, daily administration of 40 mg/kg IU1 to mice markedly reduced the subcutaneous tumor volume of hepatocellular carcinoma [21], decreased the number of liver metastases from pancreatic ductal adenocarcinoma [35] and increased the sensitivity of breast cancer to enzalutamide treatment [23]. In the nervous system, intraperitoneal injections of 400 μg/kg IU1 or direct intracranial injections of 12 μg IU1 have also been shown to protect against ischemic neuronal injury [22, 42]. Our study suggested that intraperitoneal injection of IU1 notedly improved D-gal-induced follicle reduction in mice and reduced ETO-induced DNA damage in granulosa cells, further indicating that USP14 may serve as a therapeutic target for POI. In recent years, several USP14 inhibitors have been developed, such as IU1-47, IU1-206 and IU1-248, which are 10-fold more potent than IU1 and may be more effective drugs for POI treatment in the future [15].

Our study showed that USP14 may cause DNA damage in granulosa cells by affecting the expression and function of proteins such as RNF168, Ku70 and DDB1, of which USP14-mediated ubiquitination of RNF168 and Ku70 has been reported [16, 17]. DDB1 is a component of the Cullin4A (CUL4A)-DDB1 complex, which is a type of zinc-ring ubiquitin ligase (CUL4A-ring ubiquitin 3-ligases, CRL4). As an adaptor protein, DDB1 connects CUL4A with CUL4-associated factors (DCAFs), forming more than 90 E3 ligases. CRL4 mainly regulates the degradation of proteins involved in DDR and cell cycle regulation. DDB1 was first found to be involved in NER, and recessive mutations in the DDB1 gene can lead to the development of xeroderma pigmentosum (XP), which is characterized by high skin sensitivity to UV radiation and susceptibility to skin cancer [28, 43]. When cells are subjected to UV radiation, the DDB1/DDB2 complex is activated to recognize histones, mediating their ubiquitination and degradation, which in turn induces chromatin remodeling, recruits XP group C (XPC) proteins to the damaged site, and initiates the NER pathway [44]. DDB1 is also involved in UV-induced gene transcription. For example, this molecule mediates the transcription of matrix metalloproteinase 13 (MMP13), a member of the protein hydrolase family involved in extracellular matrix remodeling and senescence-associated interstitial fibrosis [28]. The transcription factor activity of DDB1 is also closely related to cellular senescence, with DDB1-mediated transcriptional activity significantly lower in growing cells than in senescent cells [45]. E2F1 is a key transcription factor for regulating the cell cycle and is negatively regulated by DDB1, which may be associated with DNA damage-induced cell cycle arrest [46]. In addition, the CUL4A-DDB1-CDT2 ubiquitin ligase regulates the interaction between PCNA and MDM2, resulting in low protein levels of p53 in normal cells by inducing polyubiquitinated degradation. DDB1 is also involved in mediating ubiquitinated degradation of the p21 protein and the interaction between p21 and PCNA. Overall, upregulated USP14 decreased both the expression and ubiquitination levels of DDB1, likely through the aforementioned molecular mechanisms, thereby impeding DDR and promoting cellular senescence in granulosa cells [47].

Conclusions

In this study, we found that the expression of USP14 is upregulated in the hLGCs of patients with bPOI, and its expression may be negatively correlated with ovarian reserve function. In addition, upregulated USP14 may impair DDR function and induce cellular senescence in granulosa cells by reducing the expression levels and ubiquitination of RNF168, Ku70 and DDB1. More importantly, the USP14 inhibitor IU1 showed promising

therapeutic effects in the D-gal-induced POI model mice with significantly improved phenotypes. In summary, the elevated expression level of USP14 in ovarian granulosa cells may contribute to the pathogenesis of POI, and targeting USP14 may be a potential therapy strategy for POI in the future.

Supplementary Information

The online version contains supplementary material available at https://doi.org/10.1186/s12967-024-05636-3.

Supplementary Material 1

Acknowledgements
We gratefully acknowledge all the staff of the Center for Reproductive Medicine, Department of Gynecology and Obstetrics, Nanfang Hospital, Southern Medical University for their support and cooperation.

Authors' contributions
XY-Z, LZ-M and SL-C conceived and designed the entire project. OW and YH-L collected the clinical samples. XY-Z, OW and YH-L performed the cell experiments. LZ-M, OW and YH-L contributed to the animal experiments. XY-Z, JZ and XF-Z analyzed the data. LZ-M, XY-Z and SL-C wrote the manuscript. All authors have read and approved the manuscript.

Funding
This work was supported by the National Natural Science Foundation of China (grant numbers: 82201794), the China Postdoctoral Science Foundation (grant numbers: 2022M711523), the Guangdong Basic and Applied Basic Research Foundation (grant number: 2021A1515111023 and 2023A1515220065).

Data availability
All data that support the findings of this study are available within the article and its supplementary materials, and raw data are available from the corresponding author upon reasonable request.

Declarations

Ethics approval and consent to participate
The study of human luteinized granulosa cell samples was approved by the Ethics Committee of Nanfang Hospital, Southern Medical University (NFEC-2017-197), and was carried out in accordance with the Declaration of Helsinki. All animal procedures were approved by the Animal Use and Care Ethics Committee of Nanfang Hospital, Southern Medical University, and were complied with the National Institutes of Health Guide for the Care and Use of Laboratory Animals.

Competing interests
The authors declare that they have no conflict of interest.

Author details
[1]Center for Reproductive Medicine, Department of Gynecology and Obstetrics, Nanfang Hospital, Southern Medical University, No. 1838 Guangzhou Northern Road, Guangzhou, Guangdong 510515, China
[2]Department of Reproductive Medicine Centre, Guangzhou First People's Hospital, South China University of Technology, No. 1 Panfu Road, Guangzhou, Guangdong 510180, China

Received: 14 April 2024 / Accepted: 27 August 2024
Published online: 11 September 2024

References

1. Jiao X, Zhang H, Ke H, Zhang J, Cheng L, Liu Y, Qin Y, Chen ZJ. Premature ovarian insufficiency: phenotypic characterization within different etiologies. J Clin Endocrinol Metab. 2017;102(7):2281–90.
2. Huang QY, Chen SR, Chen JM, Shi QY, Lin S. Therapeutic options for premature ovarian insufficiency: an updated review. Reprod Biol Endocrinol. 2022;20(1):28.
3. Gonfloni S, Jodice C, Gustavino B, Valentini E. DNA damage stress response and follicle activation: signaling routes of mammalian Ovarian Reserve. Int J Mol Sci. 2022;23(22):14379.
4. Yang Q, Mumusoglu S, Qin Y, Sun Y, Hsueh AJ. A kaleidoscopic view of ovarian genes associated with premature ovarian insufficiency and senescence. FASEB J. 2021;35(8):e21753.
5. Wang X, Zhang X, Dang Y, Li D, Lu G, Chan WY, Leung PCK, Zhao S, Qin Y, Chen ZJ. Long noncoding RNA HCP5 participates in premature ovarian insufficiency by transcriptionally regulating MSH5 and DNA damage repair via YB1. Nucleic Acids Res. 2020;48(9):4480–91.
6. Li D, Xu W, Wang X, Dang Y, Xu L, Lu G, Chan WY, Leung PCK, Zhao S, Qin Y. lncRNA DDGC participates in premature ovarian insufficiency through regulating RAD51 and WT1. Mol Ther Nucleic Acids. 2021;26:1092–106.
7. Dang Y, Wang X, Hao Y, Zhang X, Zhao S, Ma J, Qin Y, Chen ZJ. MicroRNA-379-5p is associate with biochemical premature ovarian insufficiency through PARP1 and XRCC6. Cell Death Dis. 2018;9(2):106.
8. Zhang X, Dang Y, Liu R, Zhao S, Ma J, Qin Y. MicroRNA-127-5p impairs function of granulosa cells via HMGB2 gene in premature ovarian insufficiency. J Cell Physiol. 2020;235(111):8826–38.
9. Campisi J, Fagagna F. Cellular senescence: when bad things happen to good cells. Nat Rev Mol Cell Biol. 2007;8(9):729–40.
10. Di MR, Krizhanovsky V, Baker D, d'Adda, dF. Cellular senescence in aging: from mechanisms to therapeutic opportunities. Nat Rev Mol Cell Biol. 2021;22(2):75–95.
11. Sun D, Wang Y, Sun N, Jiang Z, Li Z, Wang L, Yang F, Li W. LncRNA DANCR counteracts premature ovarian insufficiency by regulating the senescence process of granulosa cells through stabilizing the interaction between p53 and hNRNPC. J Ovarian Res. 2023;16(1):41.
12. Huang Y, Hu C, Ye H, Luo R, Fu X, Li X, Huang J, Chen W, Zheng Y. Inflamm-Aging: A New Mechanism Affecting Premature Ovarian Insufficiency. J Immunol Res. 2019; 2019: 8069898.
13. He L, Wang X, Cheng D, Xiong Z, Liu X. Ginsenoside Rg1 improves pathological damages by activating the p21-p53-STK pathway in ovary and Bax-Bcl2 in the uterus in premature ovarian insufficiency mouse models. Mol Med Rep. 2021; 23(1): 37.
14. Wang D, Ma H, Zhao Y, Zhao J. Ubiquitin-specific protease 14 is a new therapeutic target for the treatment of diseases. J Cell Physiol. 2021;236(5):3396–405.
15. Wang F, Ning S, Yu B, Wang Y. USP14: structure, function, and Target Inhibition. Front Pharmacol. 2022;12:801328.
16. Sharma A, Alswillah T, Singh K, Chatterjee P, Willard B, Venere M, Summers MK, Almasan A. USP14 regulates DNA damage repair by targeting RNF168-dependent ubiquitination. Autophagy. 2018;14(11):1976–90.
17. Sharma A, Alswillah T, Kapoor I, Debjani P, Willard B, Summers MK, Gong Z, Almasan A. USP14 is a deubiquitinase for Ku70 and critical determinant of non-homologous end joining repair in autophagy and PTEN-deficient cells. Nucleic Acids Res. 2020;48(2):736–47.
18. Sharma A, Almasan A. USP14 regulates DNA damage response and is a target for Radiosensitization in Non-small Cell Lung Cancer. Int J Mol Sci. 2020;21(17):6383.
19. Shi D, Wu X, Jian Y, Wang J, Huang C, Mo S, Li Y, Li F, Zhang C, Zhang D, et al. USP14 promotes tryptophan metabolism and immune suppression by stabilizing IDO1 in colorectal cancer. Nat Commun. 2022;13(1):5644.
20. Li Y, Liu YD, Zhou XY, Zhang J, Wu XM, Yang YZ, Chen YX, Zhang XF, Li X, Ma LZ, et al. Let-7e modulates the proliferation and the autophagy of human granulosa cells by suppressing p21 signaling pathway in polycystic ovary syndrome without hyperandrogenism. Mol Cell Endocrinol. 2021;535:111392.
21. Lv C, Wang S, Lin L, Wang C, Zeng K, Meng Y, Sun G, Wei S, Liu Y, Zhao Y. USP14 maintains HIF1-α stabilization via its deubiquitination activity in hepatocellular carcinoma. Cell Death Dis. 2021;12(9):803.
22. Min JW, Lü L, Freeling JL, Martin DS, Wang H. USP14 inhibitor attenuates cerebral ischemia/reperfusion-induced neuronal injury in mice. J Neurochem. 2017;140(5):826–33.
23. Xia X, Huang C, Liao Y, Liu Y, He J, Guo Z, Jiang L, Wang X, Liu J, Huang H. Inhibition of USP14 enhances the sensitivity of breast cancer to enzalutamide. J Exp Clin Cancer Res. 2019;38(1):220.
24. Lee BY, Han JA, Im JS, Morrone A, Johung K, Goodwin EC, Kleijer WJ, DiMaio D, Hwang ES. Senescence-associated beta-galactosidase is lysosomal beta-galactosidase. Aging Cell. 2006;5(2):187–95.

25. Lee YR, Kang GS, Oh T, Jo HJ, Park HJ, Ahn GO. DNA-Dependent protein kinase Catalytic Subunit (DNA-PKcs): beyond the DNA double-strand break repair. Mol Cells. 2023;46(4):200–5.
26. Sharma N, Zhu Q, Wani G, He J, Wang QE, Wani AA. USP3 counteracts RNF168 via deubiquitinating H2A and γH2AX at lysine 13 and 15. Cell Cycle. 2014;13(1):106–14.
27. Liu B, Jiang S, Li M, Xiong X, Zhu M, Li D, Zhao L, Qian L, Zhai L, Li J, et al. Proteome-wide analysis of USP14 substrates revealed its role in hepatosteatosis via stabilization of FASN. Nat Commun. 2018;9(1):4770.
28. Iovine B, Iannella ML, Bevilacqua MA. Damage-specific DNA binding protein 1 (DDB1): a protein with a wide range of functions. Int J Biochem Cell Biol. 2011;43(12):1664–7.
29. Dasovich M, Leung AKL. PARPs and ADP-ribosylation: deciphering the complexity with molecular tools. Mol Cell. 2023;23:253–8.
30. Rostami DM, Noroozzadeh M, Mosaffa N, Zadeh-Vakili A, Piryaei A, Ramezani Tehrani F. Induced premature ovarian insufficiency by using D galactose and its effects on reproductive profiles in small laboratory animals: a systematic review. J Ovarian Res. 2019;12(1):96.
31. Wang YL, Wu WR, Lin PL, Shen YC, Lin YZ, Li HW, Hsu KW, Wang SC. The functions of PCNA in Tumor Stemness and Invasion. Int J Mol Sci. 2022;23(10):5679.
32. Shen QQ, Jv XH, Ma XZ, Li C, Liu L, Jia WT, Qu L, Chen LL, Xie JX. Cell senescence induced by toxic interaction between α-synuclein and iron precedes nigral dopaminergic neuron loss in a mouse model of Parkinson's disease. Acta Pharmacol Sin. 2024;45(2):268-81
33. Ding X, Gong X, Fan Y, Cao J, Zhao J, Zhang Y, Wang X, Meng K. DNA double-strand break genetic variants in patients with premature ovarian insufficiency. J Ovarian Res. 2023;16(1):135.
34. Huang X, Luan B, Wu J, Shi Y. An atomic structure of the human 26S proteasome. Nat Struct Mol Biol. 2016;23(9):778–85.
35. Zhao C, Gong J, Bai Y, Yin T, Zhou M, Pan S, Gao Y, Zhang Z, Shi Y, Zhu F, et al. A self-amplifying USP14-TAZ loop drives the progression and liver metastasis of pancreatic ductal adenocarcinoma. Cell Death Differ. 2023;30(1):1–15.
36. Ge J, Wang Y, Chen X, Yu K, Luo ZQ, Liu X, Qiu J. Phosphoribosyl-linked serine ubiquitination of USP14 by the SidE family effectors of Legionella excludes p62 from the bacterial phagosome. Cell Rep. 2023;42(8):112817.
37. He FT, Fu XL, Li MH, Fu CY, Chen JZ. USP14 regulates ATF2/PIK3CD Axis to promote microvascular endothelial cell proliferation, Migration, and Angiogenesis in Diabetic Retinopathy. Biochem Genet. 2023;61(5):2076–91.
38. Perry JW, Ahmed M, Chang KO, Donato NJ, Wobus DSH. Antiviral activity of a small molecule deubiquitinase inhibitor occurs via induction of the unfolded protein response. PLoS Pathog. 2012;8(7):e1002783.
39. Domanska UM, Kruizinga RC, Nagengast WB, Timmer-Bosscha H, Huls G, de Vries EG, Walenkamp AM. A review on CXCR4/CXCL12 axis in oncology: no place to hide. Eur J Cancer. 2013;49(1):219–30.
40. Liao Y, Xia X, Liu N, Cai J, Guo Z, Li Y, Jiang L, Dou QP, Tang D, Huang H, et al. Growth arrest and apoptosis induction in androgen receptor-positive human breast cancer cells by inhibition of USP14-mediated androgen receptor deubiquitination. Oncogene. 2018;37(14):1896–910.
41. Crimmins S, Sutovsky M, Chen PC, Huffman A, Wheeler C, Swing DA, Roth K, Wilson J, Sutovsky P, Wilson S. Transgenic rescue of ataxia mice reveals a male-specific sterility defect. Dev Biol. 2009;25(1):33–42.
42. Doeppner TR, Doehring M, Bretschneider E, Zechariah A, Kaltwasser B, Müller B, Koch JC, Bähr M, Hermann DM, Michel U. MicroRNA-124 protects against focal cerebral ischemia via mechanisms involving Usp14-dependent REST degradation. Acta Neuropathol. 2013;126(2):251–65.
43. Yurchenko AA, Rajabi F, Braz-Petta T, Fassihi H, Lehmann A, Nishigori C, Wang J, Padioleau I, Gunbin K, Panunzi L, et al. Genomic mutation landscape of skin cancers from DNA repair-deficient xeroderma pigmentosum patients. Nat Commun. 2023;14(1):2561.
44. Wang QE, Zhu Q, Wani G, Chen J, Wani AA. UV radiation-induced XPC translocation within chromatin is mediated by damaged-DNA binding protein, DDB2. Carcinogenesis. 2004;25(6):1033–43.
45. Bevilacqua MA, Iovine B, Zambrano N, D'Ambrosio C, Scaloni A, Russo T, Cimino F. Fibromodulin gene transcription is induced by ultraviolet irradiation, and its regulation is impaired in senescent human fibroblasts. J Biol Chem. 2005;280(36):31809–17.
46. Nichols AF, Itoh T, Zolezzi F, Hutsell S, Linn S. Basal transcriptional regulation of human damage-specific DNA-binding protein genes DDB1 and DDB2 by Sp1, E2F, N-myc and NF1 elements. Nucleic Acids Res. 2003;31(2):562–9.
47. Abbas T, Sivaprasad U, Terai K, Amador V, Pagano M, Dutta A. PCNA-dependent regulation of p21 ubiquitylation and degradation via the CRL4Cdt2 ubiquitin ligase complex. Genes Dev. 2008;22(18):2496–506.

Publisher's note